Thermal Balance and Water Ice Sublimation on the Surface of Hyperactive Comet 103P/Hartley2

Yuxian Yue*[1], Jiancen Liu[1], Xiaohui Wang[1]

[1]School of Astronautics, Beihang University, Beijing, China.

Corresponding author: Yuxian Yue (sy1715318@buaa.edu.cn)

Key Points:

- This paper shows that water ice sublimation has a significant effect on the surface thermodynamic equilibrium of comet nuclei.
- This paper proposes a new understanding of the high water production rate observed on hyperactive comets.
- Methods of spectral fitting and analysis are applied, including a solution to the Fredholm equation in black-body radiation inverse problem.

Plain Language Summary

This paper analyzed the effect of water ice sublimation on the surface thermal balance of 103P comet nucleus. According to the roughness model and the law of water ice sublimation, the water production rate and water ice sublimation temperature on the comet nucleus surface are inferred.

Abstract

Hyperactive comets have attracted attention due to their high water production rate with an unclear mechanism, though some hypotheses are proposed to explain it. Based on the thermal theories of the comet nuclei, this paper studied a comet surface thermal model considering the sublimation of H_2O. In this paper, a method for solving the sublimation rate of water ice by infrared spectra is proposed. The method adopts the assumption of comet nucleus surface temperature roughness and uses the numerical solution of the Fredholm equation. We use the HRI-IR spectrum (1.05-4.8 μm) data by EPOXI to analyze the pixel water sublimation rate of hyperactive comet 103P/Hartley2. The results show that sublimation exists in most areas of the surface with or without surface roughness, and most of the water production rate (70% ~ 90%) may come from the comet nucleus. According to the sublimation law, it is estimated that the sublimation temperature of water ice on 103P is above 180K. If the dust-to-ice volume ratio is 3:1, the sublimation temperature is about 200-210K, which indicates that the water ice may sublimate underneath. This may explain why exposed water ice on the surface can hardly be observed while the active fraction of this comet is up to 100%.

1 Introduction

1.1 Theory of comet nucleus

According to the comet nucleus theory proposed by Whipple et al. (1951) and studies of an uncounted number of researchers, the volatiles (mainly water ice, dry ice, and other oxides represented by NO_x) on the surface of the comet nucleus sublimates rapidly when the comet moves close to the sun, causing the refractory dust particles to escape, thus forming coma and tail structures. Huebner et al. (2006) systematically summarized the physical characteristics of the comet nucleus, providing a nucleus model and theoretical basis for subsequent researches. The sublimation of volatiles significantly affects the thermal balance on the surfaces of cometary nuclei, since the sublimation rate of the fusible solid is very sensitive to temperature in extremely low gas pressure. The academic has been studying how the volatiles sublimate.

Squires and Beard (1961) first studied the thermal balance of the comet nuclei and proposed a method for the study of surface thermodynamics. Following this theory, a series of studies about the thermodynamics of comet nuclei are carried out by many researchers (e.g., Weissman et al., 1981; Kührt, 1981; Prialnik, 1989; Julian et al., 2000; Gutierrez et al., 2001). The matter stage change and gas flow on the comet nucleus dominated by the thermodynamic state is also widely studied (e.g., Fanale et al., 1984; Benkhoff et al., 1996; Gortsas et al., 2011; Keller et al., 2015; Hu et al., 2017).

Lebofsky et al. (1986) proposed the Standard Thermal Model (STM) based on solar radiation and black body radiation which is widely used in planetary science. Spencer et al. (1989) proposed the concept of the thermal inertia of small celestial bodies based on STM and the surface heat conduction model of small celestial bodies, including the comet nuclei. Considering the sublimation of volatiles (mainly water ice) on the comet nuclei, Groussin et al. (2004) established a simplified water ice fraction model, assuming that the nucleus is an ideal sphere and the thermal inertia is zero. Following this model, Groussin et al. (2007,2013), and Davidsson et al. (2009,2012,2015) measured the brightness temperature of 9P, 103P using the Deep Impact and EPOXI near-infrared spectrometer data, as well as 67P and some asteroids from Rosetta, and proposed the concept of surface roughness parameter (the anisothermal

parameter) to describe the difference between the brightness temperature spectra and the observed spectra of the nuclei. However, the relationship between the temperature roughness caused by the surface topographic roughness and the sublimation of volatiles on the comet nucleus remains to be studied.

1.2 Hyperactive comet 103P/Hartley2

Comet 103P/Hartley2 is characterized by its small comet nucleus (average radius ~ 600m) and high water production rate (~ 10^{28} molec/s at 1.06 AU), attracting the attention of researchers. According to the approximate model of Groussin et al. (2004), the active area fraction of water ice on its surface is up to ~ 100%. This kind of comet with a high theoretical active fraction is called hyperactive comet by the community. However, when the EPOXI spacecraft visited this comet in 2010, exposed water ice is hardly detected on its surface (A'Hearn et al., 2011), which challenges some established models and assumptions, and brings new discussions.

Meech et al. (2011) estimated that more than 90% of the Hartley 2 water originates from extended sources in the coma according to the high water-ice fraction surface model. An icy dust theory was then postulated by Fougere et al. (2013) to explain its high water production rate, suggesting that water is mainly sublimated from pure ice grains in the coma. The model proposed by Kelley et al. (2013) shows that the water production rate brought by pure ice particles with a radius of 30cm is estimated to be 0.03-0.2% of the total water production rate of comets, while this proportion is 30-200% for loose icy dust bulks with a radius up to 4m. Protopapa et al. (2014) derived a lower limit of the sublimation rate from the icy dust particles in the inner coma about 0.00046±0.00001 kg/s with unknown particle size. Whether the water is mainly sublimated from icy dust is still uncertain.

On the other hand, Bonev et al. (2013) suggested that there are two sources of gaseous water in the inner coma based on the observed thermal state of water vapor, which indicated that no more than 20% of water is sublimated from icy grains. Harker et al. (2018) also showed that the main component of 103P's dust particles is amorphous materials mainly composed of carbon, and no direct evidence of water ice in the dust was found. Yue et al. (2021) performed a dynamic simulation on the spatial distribution of 103P's dust coma. Their results show that the large-scale spatial distribution of comet dust is hardly affected by water ice sublimation. More recent research by Protopapa et al. (2021) also suggested that there is no evidence for the existence of water-ice grains in the coma of another hyperactive comet, 46P/Wirtanen, based on ground-based observations.

All those results indicate that the water ice grains ejected into the coma may not be the only reason for the hyperactivity of some comets. The "hyperactive" nature of 103P is yet to be fully understood.

1.3 A new method: fitting sub-pixel temperature by solving inverse problem of black body radiation

This paper reconstructed the thermodynamic model and analysis of 103P following Groussin et al.'s research (2004 and 2009), using the HRI-IR (High Resolution Instrument - InfraRed) data from EPOXI(DIXI) mission.

In this paper, the assumption of temperature roughness is adopted, and the distribution of sub-pixel surface temperature of 103P is fitted using the infrared spectral data. This fitting is a typical inverse problem of black body radiation, which has been systematically studied by

Bojarsky (1982), Chen et al. (1990), Dai et al. (1992) and numerically solved by Ji et al. (2006, 2011). In this paper, the Fredholm integral equation, the core equation of the problem, is solved by using the basis function fitting method, and the approximate distribution of the temperature in the sub-pixel level is obtained. Using this distribution, the energy absorbed by the sublimation of water ice on the surface can be calculated based on the energy balance equations, and the corresponding surface sublimation rate can then be obtained.

The total water production rate of the comet nucleus can be obtained by integrating the surface water sublimation rate. At the same time, the relationship between water ice volume ratio (according to dust-to-gas ratio) and sublimation temperature can also be established based on the gas law, and the actual sublimation temperature of water ice on 103P surface can be inferred.

This study considers the 3-D shape and dynamic model of the nucleus. The shape model is from the research of Thomas et al. (2013) and the rotation model is from Belton et al. (2013). The DEM is from Farnham et al. (2012).

2 The thermal model on the comet nucleus surface

Based on the thermodynamic model of the surface of a small celestial body by Spencer et al. (1989), the surface of the small celestial body satisfies the one-dimensional conductive heat flow equation when there is no volatile sublimation:

$$\rho C \frac{\partial T(x,t)}{\partial t} = \frac{\partial}{\partial x}\left(\kappa \frac{\partial T(x,t)}{\partial x} \right) \tag{1}$$

Where T is temperature, x is surface depth, t is time, ρ is density, C is specific heat capacity, and κ is thermal conductivity.

The thermal balance of the surface point (x=0) is considered to be mainly determined by solar radiation (considering albedo), black-body radiation, and heat conduction. Therefore the boundary condition on the surface is:

$$\left(\kappa \frac{\partial T(x,t)}{\partial x} \right)_{x=0} = \varepsilon \sigma T^4(0,t) - (1-A)F_S(t) \tag{2}$$

Where A is the bolometric Bond albedo, and F_s is the time-dependent flux of incident sunlight. σ is the Stefan-Boltzmann constant. ε is the bolometric emissivity.

For a surface that experiences periodic heat input, such as the surface of a rotating cometary nucleus, the periodic temperature variation decreases exponentially with respect to depth. The thermal skin depth (Wesselink et al., 1948), d, represents the depth of an e-fold decrease in temperature variation. The second boundary condition is at infinite depth where the temperature gradient is 0, i.e. no heat flow. In practice, generally at a depth of D=8d, the heat flow is considered 0:

$$\left. \frac{\partial T(x,t)}{\partial x} \right|_{x=D} = 0 \tag{3}$$

With the above boundary conditions, the heat conduction equation can be numerically integrated, and the variation of the temperature on the surface over time can be obtained. This variation is related to a coefficient $\Gamma=(\kappa\rho C)^{0.5}$, termed thermal inertia.

For asteroids without sublimation, the STM (standard thermal model) proposed by Lebofsky and Spencer (1989) can be used to establishing the surface thermal model. Considering an asteroid with a flat surface, the thermal balance (in W/m^2) of the surface can be as

$$I_{sun} = I_{REFF} + \dot{E} + P \tag{4}$$

In which I_{sun} is the solar radiation, I_{REFF} is the reflex (mainly decided by Bond albedo), $\dot{E}$ is the heat conduction efficiency, and P is the Planck radiation of the surface. Because the surface is summed to be flat, P is actually the black-body radiation corresponding to the surface temperature. According to the STM, the thermodynamic model of 103P without water ice sublimation and surface roughness can be established. Figure 1 shows the temperature distribution on the surface based on the DEM of 103P. (The detailed model and data can be found in the repository of this paper.)

The thermal inertia Γ is approximated to 50 W/K/m^2/s$^{1/2}$ according to Groussin et al. 2013's research. The albedo used in the model is 0.04 according to Li et al. (2013) and A' Hearn et al. (2011). The heliocentric distance is 1.06AU.

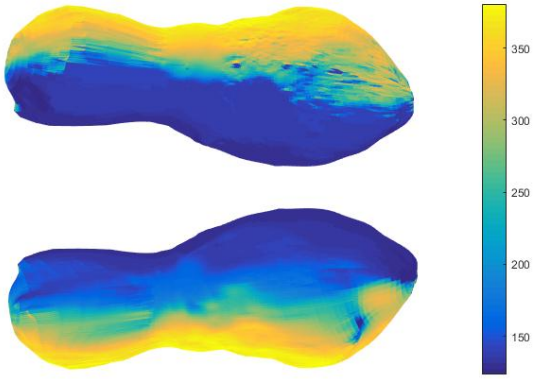

Fig.1 Surface temperature distribution of 103P simulated by the STM (without sublimation)

In fact, the sublimation of water ice on the comet nucleus will affect the thermodynamic process on the surface. According to the analysis of jet areas on the surface of 103P (Shi et al., 2016; Hu et al., 2017; Herny et al., 2021) and surface data of comet 67P from Rosetta (Davidsson et al., 2022, Groussin et al., 2019, Bouquety et al., 2021, Fornasier et al., 2016, De Sanctis et al., 2015), water ice may exist at a certain depth in the surface layer of the comet nucleus. The simplified thermodynamic model of the surface layer of the comet nucleus is shown in Fig.2. This model does not involve the surface roughness (or considers that the surface is small enough to be flat).

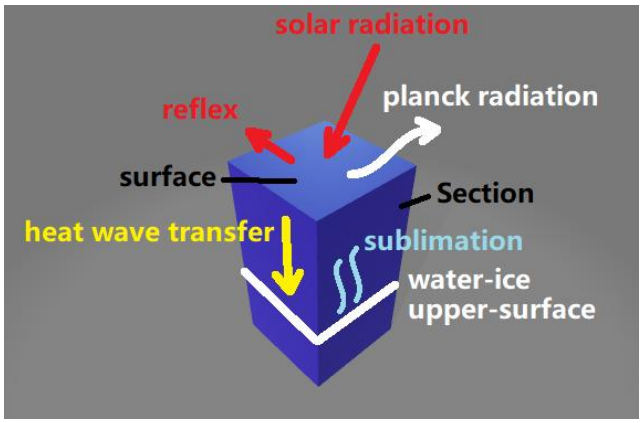

Fig.2 The simplified model of surface layer of comet nucleus

Based on the surface layer model, Eq.(5) can be obtained according to the energy balance (Huebner et al., 2006):

$$I_{sun} = I_{REFF} + \dot{E} + P' + S + E_g \tag{5}$$

In which I_{sun} is the solar radiation, I_{REFF} is the reflex (mainly decided by Bond albedo), $\dot{E}$ is the heat conduction efficiency, and P' is the actual black-body radiation of the surface with temperature roughness. S is the energy absorbed by sublimation of volatiles (mainly water ice in most areas), E_g is the heat absorption of water vapor. S and E_g include the energy of the possible re-condensation/re-sublimation.

For water ice, under low temperature (<300K) and low pressure (<1kPa), the energy changes between solid crystalline phases are always low as about 1.94 kJ/kg (McMillan et al., 1965, Yamamuro et al., 1987, Handa et al., 1988), while the energy absorbed by sublimation is about 2830 kJ/kg (Feistel et al., 2007), so S can be approximated as sublimation energy.

At the same time, the specific heat capacity of water vapor (under constant pressure) is about 1.78 kJ/kg/K/m^2（"Pure Component Properties" (Queriable database). Chemical Engineering Research Information Center. Retrieved 8 May 2007.），which is only about 170 kJ/kg when the temperature of water vapor is raised by 100K. Eg is also far less than S and can be omitted.

Therefore, the sum of S and E_g can be approximately replaced by the sublimation term:

$$S + E_g \approx \omega \cdot H \tag{6}$$

In which ω is the water ice sublimation rate from unit area surface layer, and H is the latent heat of water ice sublimation, which is nearly a constant between 100-300K, taken as 2830kJ/kg (Feistel et al., 2007) in our modeling.

Comparing Eq.(4) and Eq.(5), it can be seen that the difference between the surface black-body radiation P based on the STM and the actual surface radiation P' is mainly caused by the sublimation term:

$$P = P' + S + E_g \approx P' + \omega \cdot H \tag{7}$$

Therefore, when the theoretical radiation P has been determined according to the NEATM, the sublimation rate ω can be approximately calculated as long as the actual black-body radiation P' on the surface of the comet nucleus is obtained.

3 Process of infrared data of 103P nucleus from EPOXI mission

The Deep Impact spacecraft has provided infrared measurements of 103P using an HRI-IR (1.05–4.8 μm) spectrometer instrument (High Resolution Instrument-InfraRed spectrometer; Hampton et al., 2005). During the DIXI (Deep Impact eXtended Investigation), the Deep Impact spacecraft flies by 103P/Hartley 2 at the closest approach distance of 700 km on 4 November 2010, collecting data from this hyperactive comet. The infrared data of 103P is calibrated in 3 versions (v1.0, v2.0, and v3.0)(NASA.PDS: small bodies: EPOXI, https://pds-smallbodies.astro.umd.edu/data_sb/missions/epoxi/index.shtml. Version 3.0 includes the application of scaled master dark subtraction for DOY 307 and in scene dark subtraction for DOY 311-313, as well as the use of an average per scan optical bench temperature in the pipeline processing. Version 3 also includes the calibration enhancements implemented in Version 2 of this dataset: a new per-pixel linearity correction treatment and its propagation through the calibration steps (i.e., bad-pixel maps, flat-field file update, revised spectral calibration curve), new mode-dependent master darks, an optimized scaling factor for the master dark, and a refinement in the absolute spectral calibration curve (McLaughlin et al., 2014).

In this paper, the surface thermodynamic state of 103P was studied by using the infrared spectral data V3.0.

3.1 Hypothesis

According to the model in Section 2.1 and the research on surface roughness by Groussin et al. (2009, 2013) and Davidsson et al. (2009, 2012, 2015), we give the following assumptions: (in the single-pixel area corresponding to the observation data)

Hypothesis-1: There is temperature roughness on the comet nucleus surface, and the fraction of the area with temperature T in a pixel area is assumed to be $g(T)$. The integral of $g(T)$ under all temperatures is 1, so it can be regarded as a probability density function (PDF). Note that this surface refers to the surface area corresponding to the observation projection plane. The pixel thermal radiation of the nucleus surface observed by HIR-RI is inverse black body radiation.

Hypothesis-2: For areas with solar radiation, there is a theoretical upper limit on the surface temperature of the comet nucleus. The maximum temperature is the corresponding black-body radiation temperature (no sublimation) under direct sunlight (I_{sun0}) considering the surface roughness, set as T_H:

$$\sigma T_H^{\ 4} = I_{sun0} \tag{8}$$

Where σ is the Stefan-Boltzmann constant. For 103P at a distance of 1.06 AU from the sun, T_H is about 382K. Note that the incidence angle of the small region corresponding to T_H is 0°, so there is hardly self-heating effect in theory. The maximum temperature fitted in the study of Groussin et al. 2013 also does not exceed 370K, so it is reasonable to take 382k as the upper limit of the theoretical temperature.

Hypothesis-3: For areas receiving solar radiation, there is a lower limit for the surface temperature. The minimum temperature corresponds to areas with no sunshine and the water ice coverage reaches 100%. Therefore, the minimum temperature T_L is set as the temperature of water ice sublimation (200K, Hubner et al., 2006).

3.2 Data fitting

The pixel infrared spectrum of 103P is mainly composed of reflection spectrum and black-body radiation spectrum:

$$F(\lambda) = F_{REFF}(\lambda) + \varepsilon_d \cdot u(\lambda) \tag{9}$$

Where F is the direct observed spectrum, F_{REFF} is the reflection spectrum, ε_d is the directional emissivity, and u is the black-body radiation spectrum with sub-pixel temperature roughness.

According to Kirchhoff's law, the directional emissivity ε_d of an isotropic scatter can be derived from the reflectance factor *REFF* (Hapke, 1993):

$$\varepsilon_d = 1 - REFF = 1 - \frac{\pi F_{REFF}(\lambda)}{F_{receive}(\lambda)} = 1 - \frac{\pi F_{REFF}(\lambda)}{\cos(i) F_{sun}(\lambda) / r_h^2} \tag{10}$$

Where $F_{receive}$ is the received irradiance from the sun, i is the incidence angle, F_{sun} is the solar irradiance at 1 AU, and r_h is the heliocentric distance of the comet at the time of observation (1.06 AU for 103P).

F_{REFF} can be approximately modeled as the solar spectrum with a spectral slope S′ (in % per kÅ and derived in the spectral range1.5−2.2 μm) and normalized to the data at 1.8μm (Groussin et al., 2013).

As the observation band is limited in 1.05-4.8 μm, it is not easy to accurately fit the surface temperature distribution corresponding to the pixel through $u(\lambda)$. According to the assumption in Section 2.2.1, $u(\lambda)$ is actually a mixed spectrum of different temperatures with different area ratios (the same assumption is also made in Davidsson et al., 2015). Therefore, the pixel-level $u(\lambda)$ is:

$$u(\lambda) = \int_0^\infty g(T) B(\lambda, T) dT \tag{11}$$

Where $g(T)$ is the temperature distribution function (assumption 1 in Section 2.2.1), and B is the ideal black-body radiation. Considering hypothesis-2 and hypothesis-3 in Section 2.2.1, the upper and lower limits of T are T_H and T_L, respectively, then (11) becomes (11'):

$$u(\lambda) = \int_{T_L}^{T_H} g(T) B(\lambda, T) dT \tag{11'}$$

In this formula, u is the known data, B is the known function, and only $g(T)$ needs to be solved. This is a typical inverse problem of black-body radiation. Equation (11') is a typical Fredholm integral equation of the first kind and can be solved by numerical method. According to the research of (Ji et al., 2006, 2011), we use the method of basis function fitting. Since the function type of $g(T)$ is also unknown, we choose the piecewise function (the Floor Function) with unknown parameters as the approximate distribution function, as shown in Fig.3.

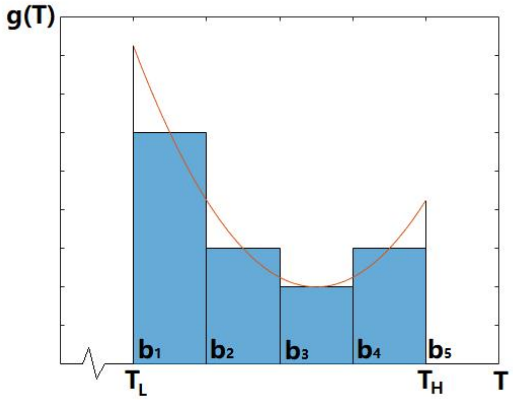

Fig.3 The Floor Function was used to fit the temperature distribution function. The horizontal axis is the temperature and the vertical axis is the probability density. The red curve in the figure is the actual distribution of *T*, and the blue function is the fitted distribution.

To balance the accuracy of fitting results and the calculation complexity, we choose the 4-floors distribution to fit $g(T)$. Considering the characteristics of the Planck function, the five boundary points of the 4 floors are:

$$\begin{aligned} b_1 &= T_L; \\ b_2 &= \sqrt[4]{\frac{T_H^{\,4} - T_L^{\,4}}{4} + T_L^{\,4}}; \\ b_3 &= \sqrt[4]{2 \cdot \frac{T_H^{\,4} - T_L^{\,4}}{4} + T_L^{\,4}}; \\ b_4 &= \sqrt[4]{3 \cdot \frac{T_H^{\,4} - T_L^{\,4}}{4} + T_L^{\,4}}; \\ b_5 &= T_H. \end{aligned} \tag{12}$$

The approximated distribution function of T is:

$$g(T)_{appr} = \begin{cases} \dfrac{x_1}{b_2 - b_1}, T \in [b_1, b_2) \\ \dfrac{x_2}{b_3 - b_2}, T \in [b_2, b_3) \\ \dfrac{x_3}{b_4 - b_3}, T \in [b_3, b_4) \\ \dfrac{x_4}{b_5 - b_4}, T \in [b_4, b_5] \end{cases}; \tag{13}$$

$$x_1 + x_2 + x_3 + x_4 = 1.$$

In fact, the anisothermal parameter Λ which takes into account the fact that the surface is rough at the sub-pixel scale (Davidsson et al., 2009, Groussion et al., 2009, 2013) means using a two-points distribution model (T_{color} is one point and 0K is another point) to fit $g(T)$, and the area fraction of T_{color} is the parameter Λ:

$$g(T)_{appr'} = \begin{cases} \Lambda, T = T_{color} \\ 0, T \neq T_{color} \end{cases} \tag{14}$$

The proposal of anisothermal parameter Λ determines the existence of temperature roughness, but taking 0K as one temperature distribution point is not accurate. Therefore, the 4-floors distribution fitting method proposed in this paper is actually an improvement based on the rationality of the hypothesis.

We used the HRI-IR data of version 3.0 (5001004a, b, and 5005001) for fitting, and obtained the temperature distribution of effective pixels. Figure 4 shows the fitting spectrum and physical information of two sampled pixels.

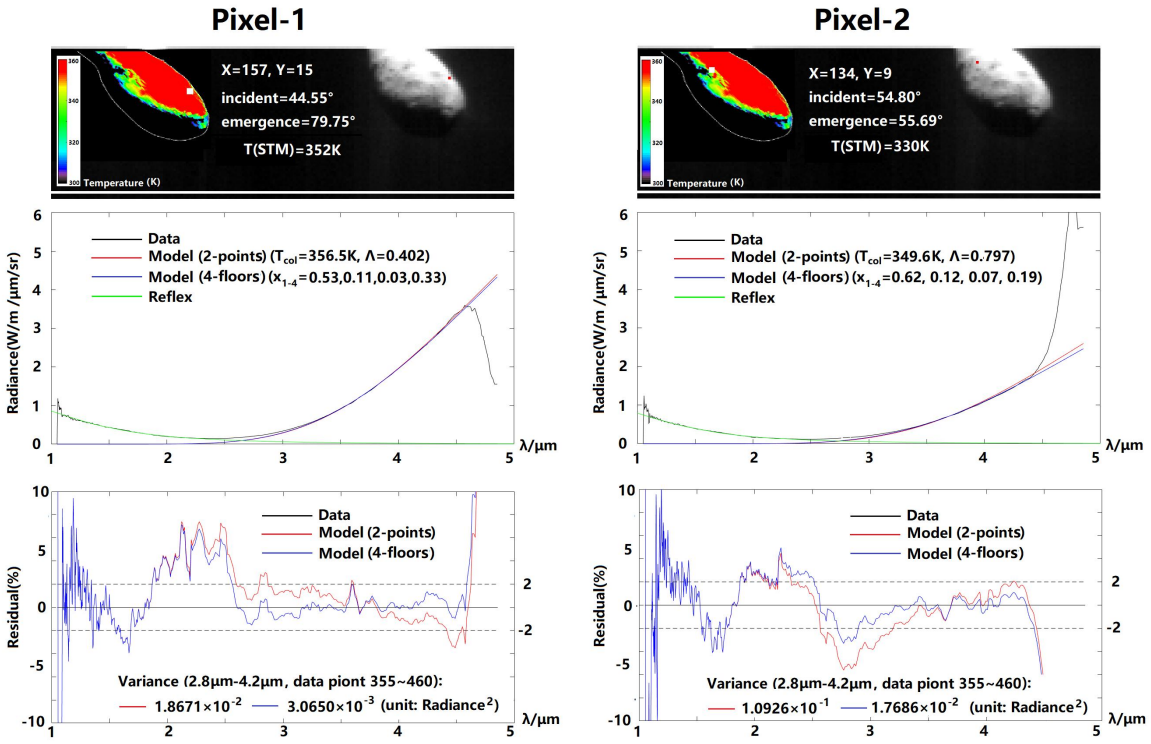

Fig.4 The spectra fitting. The left penal is pixel (15,157) and the right penal is pixel (9,134). Both pixels are from data 5001004. The top floor is the location of the pixel, the red point on the HRI-IR image (right, in 3.2 μm), and the white point on the STM temperature simulation image (left). The second floor is the fitting spectra. The third floor is the related error of the fitting. In the figure, the black curve is the observed spectra, the red curve is the fitted spectra by the 2-points model, and the blue curve is the fitted spectra by the 4-floors function model.

In most effective pixels, the spectrum fitted by the 4-floors method has smaller residuals (as well as variance) compared to that fitted by the 2-points method, while the approximate limit of residuals of both methods is about ±2%.

In order to study the effect of water ice sublimation on the surface spectrum, we also simulated the theoretical radiation spectrum without water ice sublimation. This spectrum assumes surface roughness and is derived using the surface model from Davidsson et al., 2015. The spectrum is simulated based on the incident angle, emergence angle, and azimuth angle of each pixel, using a Gaussian random roughness model with different roughnesses (5°, 20°, and 35° in Fig.5). Using this model, the theoretical radiation spectrum of each pixel without sublimation under different roughness can be obtained. It is compared with the spectrum fitted to the observation data to see how sublimation affects the surface spectrum (Fig. 6).

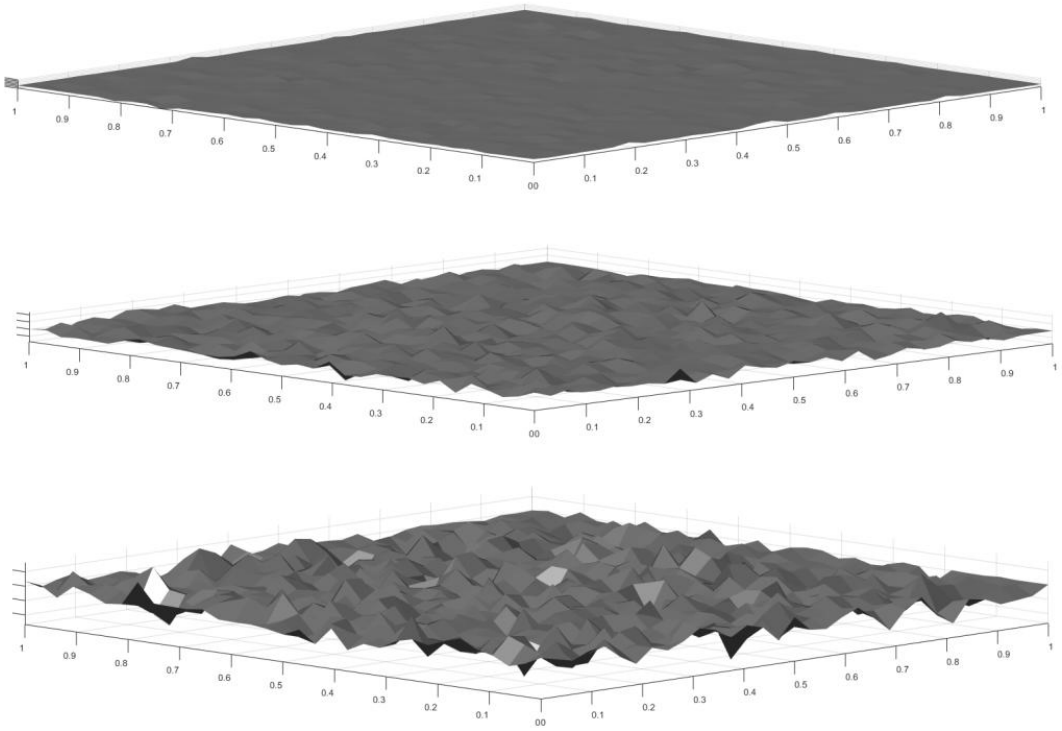

Fig.5 Surface roughness model used in this study. The model adopted Gauss random roughness and simulated 1024 facets per unit area (m^2). The roughness of the three simulated surfaces in the figure is 5°, 20°, and 35° from top to bottom.

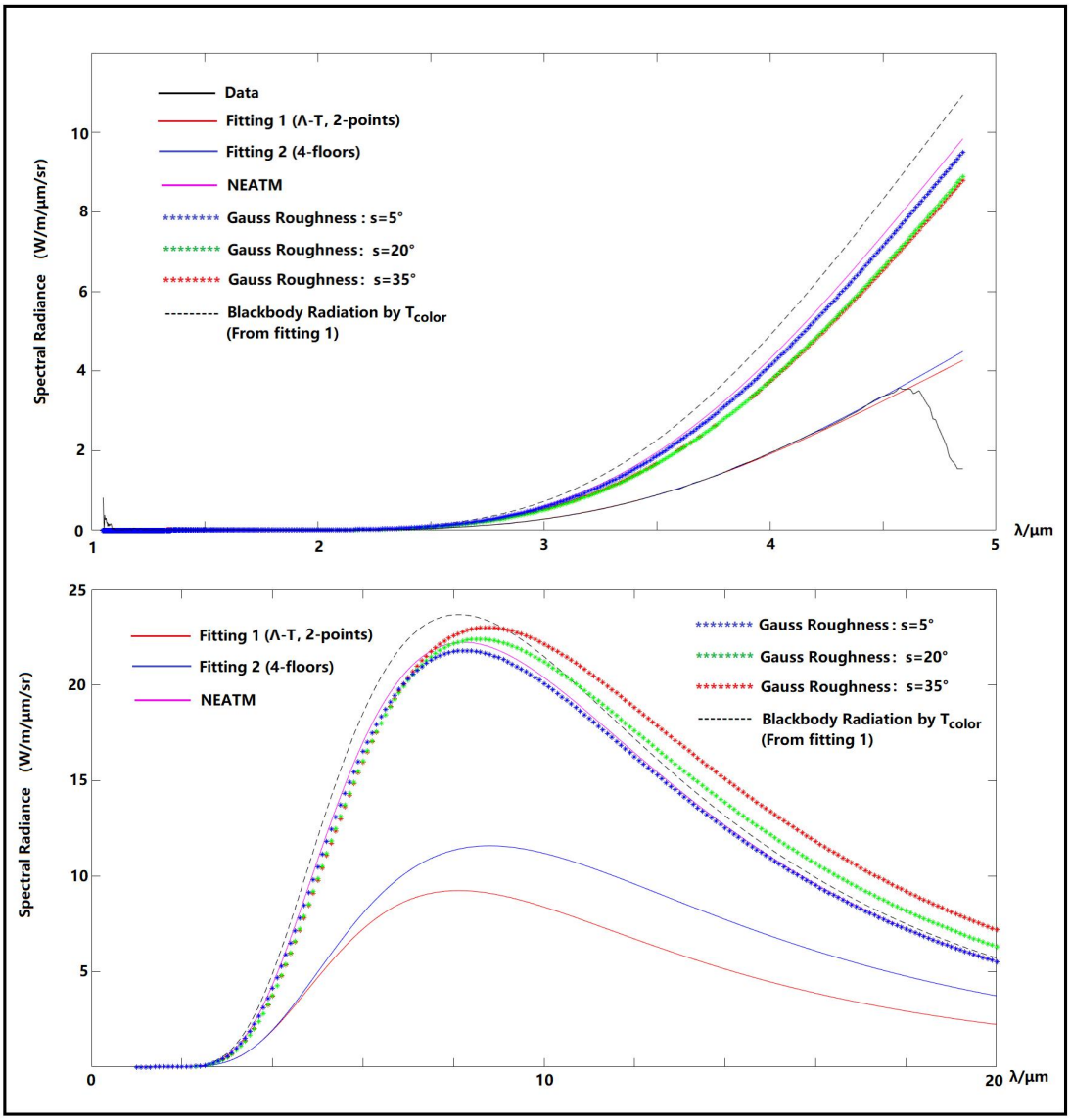
Data
Fitting 1 (Λ-T, 2-points)
Fitting 2 (4-floors)
NEATM
Gauss Roughness : s=5°
Gauss Roughness: s=20°
Gauss Roughness: s=35°
Blackbody Radiation by T_color (From fitting 1)
Spectral Radiance (W/m/μm/sr)
λ/μm
Fitting 1 (Λ-T, 2-points)
Fitting 2 (4-floors)
NEATM
Gauss Roughness : s=5°
Gauss Roughness: s=20°
Gauss Roughness: s=35°
Blackbody Radiation by T_color (From fitting 1)
Spectral Radiance (W/m/μm/sr)
λ/μm

301

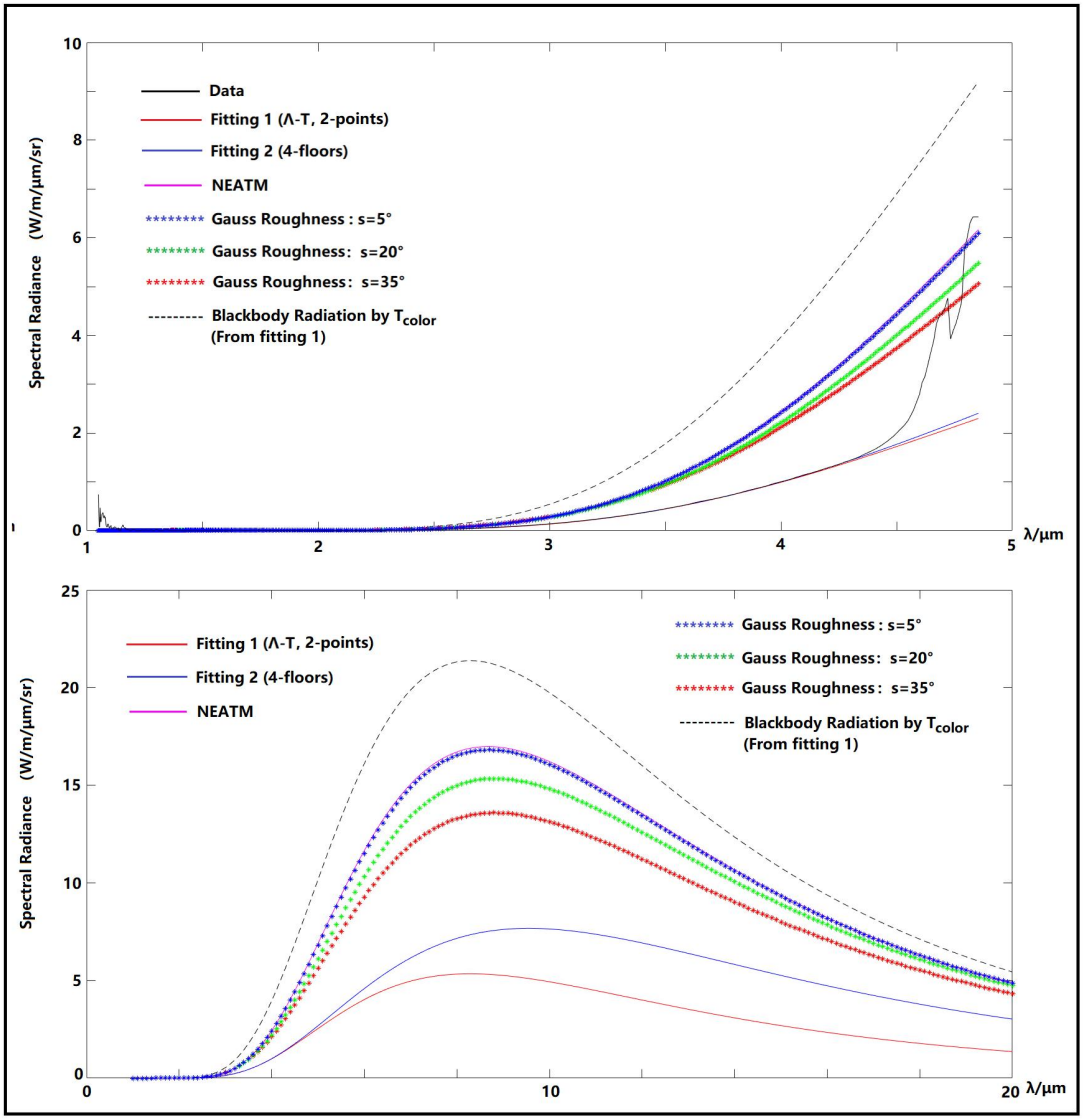

Fig.6(a,b) Spectrum only considering the surface roughness and spectrum fitted to the observed data. The first box is Pixel-1 (15,157) in Fig.4, and the second box is Pixel-2 (9,134). In each box, the upper panel is in 1-5μm, and the lower panel is in 0-20μm. In this figure, the red curve is the fitted spectrum obtained by the two-points method, the blue curve is the fitted spectrum obtained by the 4-floors method, the black curve is the observed spectrum. The purple curve is the STM model spectrum without considering the surface roughness nor sublimation. The blue, green and red dotted lines represent the spectrum of non-sublimation surfaces with roughness of 5°, 20°, and 35°, respectively. The black dashed line is the black body radiation spectrum corresponding to the fitted color temperature in the study of Groussin et al. (2013).

The surface roughness has a non-negligible influence on the real spectrum. However, based on our simulations or Davidsson's 2015 study, the surface roughness of Gauss type (or Fractal type) has an impact on the spectrum within 30%. Compared with the above simulations, the reason why the observed spectrum is significantly lower (>60%) than the STM prediction spectrum is likely to be the sublimation of water ice.

In other words, both surface roughness and water ice sublimation have a significant impact on the surface spectrum of the comet nucleus. Using the energy difference between the two types of spectrum (with and without sublimation), the energy absorbed by the sublimation of water ice can be calculated, and the relevant parameters can be further obtained.

3.3 Water sublimation rate

After obtaining an accurate temperature distribution in each pixel, we can use the Planck radiation formula to calculate the actual black-body radiation energy integral corresponding to each pixel (integration of the fitting spectrum, Model:4-floors in Fig.6):

$$P' = \int_0^{\infty}\int_{T_L}^{T_H} g(T)B(\lambda,T)dTd\lambda = \int_{T_L}^{T_H} g(T)\int_0^{\infty} B(\lambda,T)d\lambda dT \approx \int_{T_L}^{T_H} g(T)_{appr}\sigma T^4 dT \tag{15}$$

While the theoretical black-body radiation obtained by NEATM (integration of the bottom panel, s=5°, in Fig.6) is:

$$P = \sigma T_{NEATM,s}{}^4 = \int_0^{\infty} F_{NEATM,s}(\lambda)d\lambda \tag{16}$$

Then, according to Eq.(7), i.e. the sublimation efficiency is approximately the difference between P and P':

$$I_{sub} = \omega \cdot H = P - P' \tag{17}$$

the water ice sublimation rate ω corresponding to each pixel can be calculated (Fig. 5).

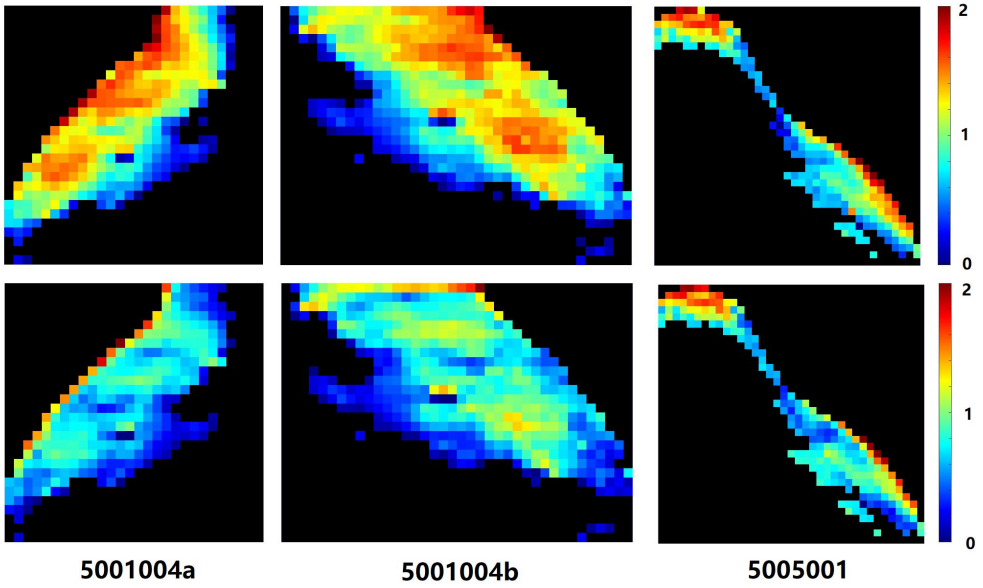

Fig.7 Water ice sublimation rate of the 103P nucleus (modeled surface roughness is 5°). The upper panel is the result by 2-points distribution fitting (T_{color} and A), and the lower panel is the result by 4-floors distribution fitting. Unit: 10^{-4} kg/s/m^2.

Figure 7 shows that there is significant water ice sublimation in most areas on the surface of the 103P comet nucleus, while areas with smaller incident angles have relatively higher sublimation rates. The active fraction of the comet is up to nearly 100% in day hemisphere, which is consistent with the conclusion in Groussin et al.'s research in 2004.

After integrating the sublimation rate of water ice in all effective pixels according to the spectrum (with roughness of 0°,5°,20°and 35°), we get the water production rate of the comet nucleus in the photo (Table.1). The relative error caused by temperature fitting in Section 3.2 is no more than 5% beside the model error.

Table.1 The water production rate from three groups of data (a: 5001004a, b: 5001004b, c: 5005001) under two fitting methods (2 pionts and 4-floors).Unit: kg/s.

Data (Method)		a (2-points)	a (4-floors)	b (2-points)	b (4-floors)	c (2-points)	c (4-floors)
Q_{eff} (kg/s)	s=0°	196.2	101.2	146.3	98.3	124.2	109.2
	s=5°	194.8	99.8	144.1	96.1	123.8	108.8
	s=20°	191.2	96.2	138.8	90.8	120.1	105.2
	s=35°	185.1	90.1	131.2	83.2	113.7	98.8
Effective Pixels		354		584		236	
Effective Area		1.0982×10^6 m^2		9.9768×10^5 m^2		1.0404×10^6 m^2	
Area Ratio*		≈0.4192		≈0.3808		≈0.3971	
Q (kg/s)	s=0°	468.0	241.5	384.2	258.1	312.8	275.0
	s=5°	464.7	238.1	378.4	252.4	311.8	274.0
	s=20°	456.1	229.5	364.5	238.4	302.4	264.9
	s=35°	441.6	214.9	344.5	218.5	286.3	248.8
Q/Q_{ob}	s=0°	156.0%	80.5%	128.1%	86.0%	104.3%	91.7%
	s=5°	154.9%	79.4%	126.1%	84.1%	103.9%	91.3%
	s=20°	152.0%	76.5%	121.5%	79.5%	100.8%	88.3%
	s=35°	147.2%	71.2%	114.8%	72.8%	95.4%	82.9%
Error bar *		±20%					

*Area ratio refers to the proportion of the area of the daytime hemisphere in the image to the total area of the daytime hemisphere of the comet nucleus (~ 0.5×5.24km^2 = 2.62km^2).

*Error bar limit refers to the maximum limit of relative error caused by surface roughness in the model. The data results under different roughnesses are under a low error bar (<20%).

This result shows that the water production rate obtained by the 4-floors fitting method is close to the observed total water production rate (~ 300kg/s, A' Hearn et al., 2011; Meech et al., 2011). This indicates that when the hypotheses in Section 2.2.1 are valid, most of the water production of 103P may come from the nucleus surface.

353

354 **4 Water sublimation of the nucleus**

355

356 In Section 3, the sublimation rate of the comet nucleus surface is already obtained using a
357 4-floors temperature fitting method. According to the gas sublimation theory, the relationship
358 between sublimation temperature and water ice coverage can be then determined. When the water ice fraction is p_w, the actual areal sublimation rate is:

$$\omega(T) = p_w \cdot \omega_0(T) \tag{18}$$

359

360 Where $\omega(T)$ is the actual water ice sublimation rate, ω_0 is the water ice sublimation rate
361 from unit pure water ice area, which is given by Knudsen's law of diffusion (Kramers et al., 1951):

$$\omega_0(T) = p_{st}(T)\sqrt{\frac{M_{gas}}{2\pi RT}} \tag{19}$$

362

363 where $p_{st}(T)$ is the saturated vapor pressure, which is given by the formula of Buck et al. (1996) as a function of temperature:

$$p_{st}(T) = \begin{cases} 611.21 \cdot \exp(\dfrac{(18.678 - t/234.5)}{258.14 + t}t), & t > 0 \\ 611.15 \cdot \exp(\dfrac{(23.036 - t/333.7)}{279.82 + t}t), & t < 0 \end{cases}, \quad t = T - 273.15 \tag{20}$$

364

365 When p_w=1, the lower limit of sublimation temperature T_{lim} can be calculated according
366 to Eq.(18-20), which is the minimum temperature required to maintain the observed water ice sublimation rate, which is about 180 ~ 200K.

367

368 A' Hearn et al. (2011), Dello Russo et al. (2011), Crovisier et al. (2013), Boissier et al.
369 (2013) derived a dust-to-gas ratio of about 2-6. Considering the mass conservation of the comet
370 nucleus, suppose that the water to dust volume ratio is 1:3, the water ice coverage of the volatile
371 layer of the comet nucleus is approximately 0.39. The approximate sublimation temperature T_{appr}
372 calculated under this circumstance is about 200 ~ 210K. The upper panel of Fig.8 is T_{lim}, and the lower panel is T_{appr}.

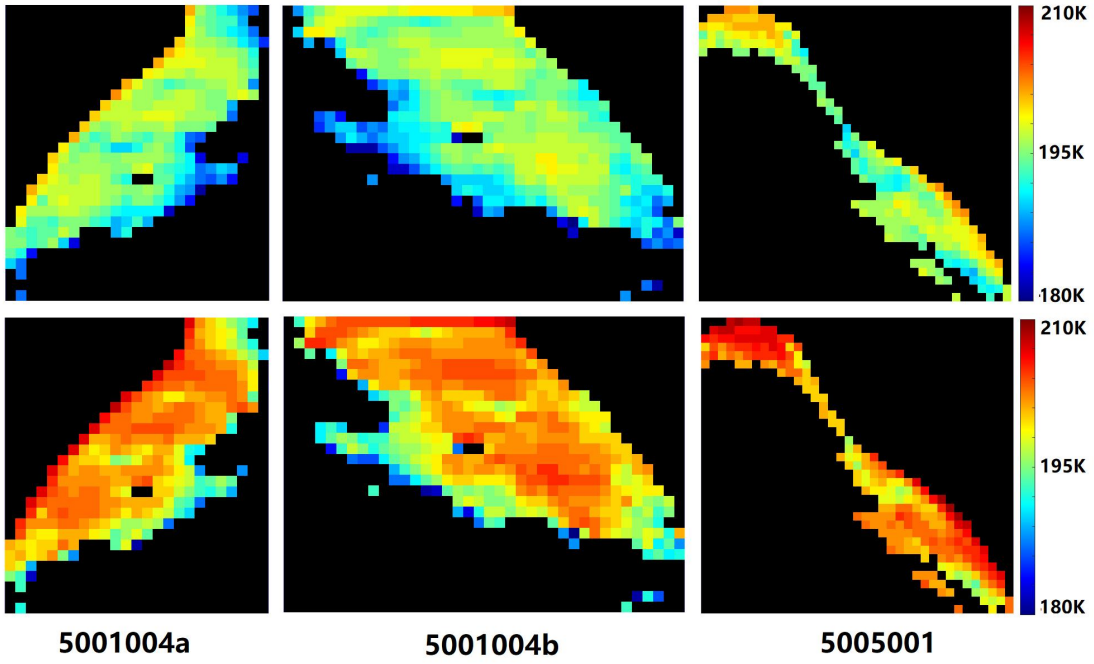

Fig.8 The sublimation temperature of water ice on 103P (surface roughness is 5°). The top panel is the minimum temperature (water ice fraction=1), while the bottom panel is the approximate temperature when the water to dust volume ratio is 1:3(water ice fraction ~0.39). Both panels are derived using the 4-floors temperature fitting method.

Such lower temperatures exist only in the dark areas or under the surface of the comet nucleus. Considering the instability of the dark areas (sometimes being illuminated), this conclusion further indicates that the water on the surface of the comet nucleus is likely to sublimate below the surface of the comet nucleus.

On the one hand, this explanation confirms the surface layer model in Section.2. On the other hand, it also explains why exposed water ice is hardly detected on the surface: most of the water ice is sublimating under the surface quietly, only exposing its existence through the energy loss of the surface infrared spectrum.

5 Conclusions

1. The approximate sub-pixel temperature distribution is solved by using the numerical solution of the inverse black-body radiation problem in this study, and the solution of Fredholm equation is fitted based on the theory of surface roughness proposed by Groussin et al. (2013) and Davidsson et al. (2015). Both surface roughness and water ice sublimation have a significant influence on the surface spectrum.

2. The sublimation rate of water ice on the surface of the comet nucleus is obtained by the energy balance equation and infrared spectrum data from the EPOXI mission. The results show that most of the water production (70% ~ 90%) of comet 103P may come from the surface of the comet nucleus according to the fitted spectrum and the surface roughness model.

3. Combined with mass conservation, it is calculated that the sublimation temperature of water ice on the 103P nucleus is higher than 180K. Assuming that the comet nucleus is isotropic and the volume ratio of gas to dust is 1:3, the approximate sublimation temperature of water ice on 103P is about 200-210K. Most of the water ice is presumed to sublimate at a certain depth underneath.

Acknowledgments

- Data availability statement：

Data in this research is processed in Matlab language.

Data and programs (version 1.0) are deposited at Dryad, naming ‘Spectrum data and thermal model of comet/103P (v1.0)’.

URL：

https://datadryad.org/stash/share/H9ABEtiwHZHO1Ean66qdfZSkqTr3_9ABm6vIR7rrCws

These data and programs are completely open.

The original datasets are from NASA’s PDS database, including:

(1)DEM of 103P.

Farnham, T.L. and Thomas, P.C., PLATE SHAPE MODEL OF COMET 103P/HARTLEY 2 V1.0, DIF-C-HRIV/MRI-5-HARTLEY2-SHAPE-V1.0, NASA Planetary Data System, 2013.

https://pdssbn.astro.umd.edu/holdings/dif-c-hriv_mri-5-hartley2-shape-v1.0/dataset.shtml

(2)HRI-IR data of 103P.

McLaughlin, S.A., B. Carcich, S.E. Sackett, K.P. Klaasen, L.M. Feaga, and S. Protopapa, EPOXI 103P/HARTLEY2 ENCOUNTER - HRII CALIBRATED SPECTRA V3.0, DIF-C-HRII-3/4-EPOXI-HARTLEY2-V3.0, NASA Planetary Data System, 2014. https://pds-smallbodies.astro.umd.edu/holdings/dif-c-hrii-3_4-epoxi-hartley2-v3.0/dataset.shtml

- Thanks：

The authors would like to thank the individual efforts and dedicated contributions of the numerous engineers and scientists who were critical in obtaining critical data on Comet 103P. We thank Li-Jianyang and O. Groussin for very helpful discussions and advice.

Open Research

The methods used and the results obtained in this paper all are publicly available.

References

A'Hearn, M.F. et al., 2011. EPOXI at Comet Hartley 2. *Science*, 332, 1396–1400.

Belton, M.J.S. et al., 2013. The complex spin state of 103P/Hartley 2: Kinematics and orientation in space. *Icarus*, 222, 595–609.

Benkhoff et al. 1996. Modeling the thermal properties and the gas flux from a porous, ice-dust body in the orbit of P/Wirtanen. *Planetary and Space Science*, 44, 665-673.

Boissier, J. et al., 2013. Gas and dust productions of comet 103P/Hartley 2 from millimetre observations: interpreting rotation-induced time variations. *Icarus*, 228, 197-216.

441 Bojarski, N. N. Inverse black body radiation. *IEEE Trans Antennas and*
442 *Propagation*,1982,30(4): 778-780.

443 Bonev, P. B. et al., 2013. Evidence for two modes of water release in Comet
444 103P/Hartley 2: Distributions of column density, rotational temperature, and ortho-para ratio.
445 *Icarus*, 222, 740–751.

446 Bouquety et al., 2021, Ancient and present surface evolution processes in the Ash region
447 of comet 67P/Churyumov-Gerasimenko. *A & A*, L649.

448 Buck A.L., 1981. Research Manual (1996) updated equation from A.L. Buck, J. *Appl.*
449 *Meteorol.*, 20, 1527.

450 Chen N., Li G. Theoretical investigation on the inverse black body radiation problem.
451 *IEEE Trans Antennas and Propagation*, 1990, 38(8): 1287-1290.

452 Crovisier, J. et al., 2013. Observations of the 18-cm OH lines of Comet 103P/Hartley 2 at
453 Nancay in support to the EPOXI and Herschel missions. *Icarus*, 222, 679–683.

454 Dai X., Dai J. On unique existence theorem and exact solution formula of the inverse
455 black-body radiation problem. *IEEE Trans Antennas and Propagation*,1992,40(3):257-260.

456 Davidsson, B.J.R. et al., 2012. Thermal inertia and surface roughness of Comet
457 9P/Tempel 1. *Icarus*, 224, 154-171.

458 Davidsson, B.J.R. et al., 2015. Interpretation of thermal emission. I. The effect of
459 roughness for spatially resolved atmosphereless bodies. *Icarus*, 252, 1–21.

460 Davidsson, B.J.R. et al., 2022. Modelling the water and carbon dioxide production rates
461 of Comet 67P/Churyumov–Gerasimenko. *Monthly Notices of the Royal Astronomical Society*,
462 509, Issue 2, 3065-3085.

463 Davidsson, B.J.R., Gutierrez, P.J., Rickman, H., 2009. Physical properties of
464 morphological units on Comet 9P/Tempel 1 derived from near-IR Deep Impact spectra. *Icarus*,
465 201, 335–357.

466 De Sanctis et al., 2015. The diurnal cycle of water ice on comet 67P/Churyumov-
467 Gerasimenko. *Nature*, 525, 500-503.

468 Dello Russo, N. et al., 2011. The volatile composition and activity of comet 103P/Hartley
469 2 during the EPOXI closest approach. *Astrophys. J.*, 734, L8.

470 Fanale, F. P., & Salvail, J. R., 1984. An idealized short-period comet model: Surface
471 insolation, H2O flux, dust flux, and mantle evolution. *Icarus*, 60, 476-511.

472 Farnham, T.L. and Thomas, P.C., PLATE SHAPE MODEL OF COMET
473 103P/HARTLEY 2 V1.0, DIF-C-HRIV/MRI-5-HARTLEY2-SHAPE-V1.0, NASA Planetary
474 Data System, 2013.

475 Feistel, R. et al., 2007. Sublimation pressure and sublimation enthalpy of H2O ice Ih
476 between 0 and 273.16 K. *Geochimica et Cosmochimica Acta*, 71, 36 - 45.

477 Fornasier et al., 2016. Rosetta's comet 67P/Churyumov-Gerasimenko sheds its dusty
478 mantle to reveal its icy nature. *Science*, 23, 354(6319):1566-1570.

479 Fougere, N. et al., 2012. Understanding measured water rotational temperatures and
480 column densities in the very innermost coma of Comet 73P/Schwassmann–Wachmann 3B.
481 *Icarus*, 221, 174–185.

482 Gortsas et al., 2011. Thermal model of water and CO activity of Comet C/1995 O1 (Hale-
483 Bopp). *Icarus*, 212, 858-866.

Groussin, O. et al., 2004. The nuclei of comets 126P/IRAS and 103P/Hartley 2. *A&A*, 419, 375–383.

Groussin, O. et al., 2007. Surface temperature of the nucleus of Comet 9P/Tempel 1. *Icarus*, 187, 16–25.

Groussin, O. et al., 2013. The temperature, thermal inertia, roughness and color of the nuclei of Comets 103P/Hartley 2 and 9P/Tempel 1. *Icarus*, 222, 580–594.

Groussin, O. et al., 2019. The Thermal, Mechanical, Structural, and Dielectric Properties of Cometary Nuclei After Rosetta. *Space Sci Rev*, (2019) 215:29.

Gutierrez et al., 2001. Effects of irregular shape and topography in thermophysical models of heterogeneous cometary nuclei. *A&A*, 374, 326-336.

Hampton, D.L. et al., 2005. An overview of the instrument suite for the Deep Impact mission. *Space Sci. Rev.*, 117, 43–93.

Handa, Y.P., et al., 1988. Energies of the phases of ice at low-temperature and pressure relative to ice Ih. *Can J Chem*, 66(4):919–924.

Harker, D. E. et al., 2018. Hyperactivity and Dust Composition of Comet 103P/Hartley 2 During the EPOXI Encounter. *The Astronomical Journal*, 155, 199–211.

Harris, A.W., 1998. A thermal model for near-Earth asteroids. *Icarus*, 131, 291–301.

Herny et al., 2021. New constraints on the chemical composition and outgassing of 67P/Churyumov-Gerasimenko. *Planetary and Space Science*, L200.

Hu et al., 2017. Thermal modelling of water activity on comet 67P/Churyumov-Gerasimenko with global dust mantle and plural dust-to-ice ratio. *MNRAS*, 469, S295–S311.

505 Huebner, W.F., 2006. Heat and Gas Diffusion in Comet Nuclei. *ISSI Science report*, SR-
506 004.

507 Ji, F. et al., 2006. A unified solution of the inverse black-body radiation problem ans
508 some exact solutions. *Inverse Problems*, 22, 1731-1737.

509 Ji, F. et al., 2011. A new solution method for black-body radiation inversion and the solar
510 area-temperature distribution. *Science China, Physics, Mechanics & Astronomy*, 54 (No.11),
511 2097-2112.

512 Julian, W.H. et al., 2000. Thermal Structure of Cometary Active Regions: Comet
513 1P/Halley. *Icarus*, 144, 160-171.

514 Keller, H.U. et al., 2015. The changing rotation period of comet 67P/Churyumov-
515 Gerasimenko controlled by its activity. *A&A*, 579, L5.

516 Kelly, M.S. et al., 2013. A distribution of large particles in the coma of Comet
517 103P/Hartley 2. *Icarus*, 222 (2): 634-652.

518 Kramers, H., 1951. The Sublimation of Ice in Vacuum. *Applied Scientific Research*, A3,
519 73–82.

520 Kührt, E., 1981. Temperature Profiles and Thermal Stresses in Cometary Nuclei. *Icarus*,
521 60, 512-521.

522 Lebofsky, L. A. et al., 1986. A refined “standard” thermal model for asteroids based on
523 observations of 1 Ceres and 2 Pallas. *Icarus*, 68, 239–251.

524 Li. J.et al., 2013. Photometric properties of the nucleus of Comet 103P/Hartley 2. *Icarus*,
525 222, 559–570.

McLaughlin, S.A., B. Carcich, S.E. Sackett, K.P. Klaasen, L.M. Feaga, and S. Protopapa, EPOXI 103P/HARTLEY2 ENCOUNTER - HRII CALIBRATED SPECTRA V3.0, DIF-C-HRII-3/4-EPOXI-HARTLEY2-V3.0, NASA Planetary Data System, 2014.

McMillan, J.A. et al., 1965. Vitreous ice - irreversible transformations during warm-up. *Nature*, 206(4986):806–807.

Meech, K.J. et al., 2011. EPOXI: Comet 103P/Hartley 2 observations from a worldwide campaign. *The Astrophysical Journal Letters*, 734: L1 (9pp).

Prialnik, 1989. Thermal evolution of cometary nuclei. *Advances in Space Research*, 9, No.3, pp.25–40.

Protopapa, S. et al., 2014. Water ice and dust in the innermost coma of comet 103P/Hartley 2. *Icarus*, 238, 191–204.

Protopapa, S. et al., 2021. Non-detection of water-ice grains in the coma of comet 46P/Wirtanen and implications for hyperactivity. *The Planetary Science Journal*, June 2021.

Shi, X et al.,2016. Sunset jets observed on comet 67P/Churyumov-Gerasimenko sustained by subsurface thermal lag. *A&A*, 586, A7.

Spencer, J.R., Lebofsky, L.A., Sykes, M.V., 1989. Systematic biases in radiometric diameter determinations. *Icarus*, 78, 337–354.

Squires and Beard, 1961. Physical and orbital behavior of comets. *ApJ*, 163, 657-667.

Thomas, P.C. et al., 2013. Shape, density, and geology of the nucleus of Comet 103P/Hartley 2. *Icarus*, 222, 550–558.

546 Weaver, H. A. et al., 1994. Detection of CO Cameron band emission in comet P/Hartley
547 2 (1991 XV) with the Hubble Space Telescope. *The Astrophysical Journal*, 422, 374–380.

548 Weissman et al., 1981. Thermal modeling of cometary nuclei. *Icarus*, 47, 302–311.

549 Wesselink, A. J. et al., 1948. Heat conductivity and the nature of the lunar surface
550 material. *Bull. Astron. Inst. Neth.*, 10, 351–363.

551 Whipple, F. L, 1951. A Comet Model. II. Physical Relations for Comets and Meteors.
552 *The Astrophysical Journal*, 113, 464–474.

553 Yamamuro, O. et al., 1987. Heat-capacity and glass-transition of pure and doped cubic
554 ices. *J. Phys. Chem. Solids*, 48(10):935–942.

555 Yue, Y. et al., 2021. Dynamic Simulation and Parameter Fitting Method of Cometary
556 Dust Based on Machine Learning. *Experimental Astronomy*, 51, 391–424.